Deeply bound π^- states in ^{207}Pb formed in the ^{208}Pb(d,^{3}He) reaction.
I. Experimental method and results

H. Gilg,* A. Gillitzer, M. Knülle, M. Münch, W. Schott, and P. Kienle
Physik-Department, Technische Universität München, D-85748 Garching, Germany

K. Itahashi, K. Oyama, and R. S. Hayano
Department of Physics, University of Tokyo, 7-3-1 Hongo, Bunkyo-ku, Tokyo 113, Japan

H. Geissel, N. Iwasa, and G. Münzenberg
Gesellschaft für Schwerionenforschung, D-64291 Darmstadt, Germany

T. Yamazaki
Institute of Particle and Nuclear Studies, High Energy Accelerator Research Organization, 3-2-1 Midori-cho, Tanashi, Tokyo 188-8501, Japan
and Japan Society for the Promotion of Science, 5-3-1 Koji-machi, Chiyoda-ku, Tokyo 102-0083, Japan

The deeply bound pionic states $(1s,2p)_{\pi^-} \otimes {}^{207}$Pb were observed for the first time, by investigating the ^{208}Pb(d,^{3}He) reaction at a beam energy of $T_d = 604.3$ MeV and at ejectile angles around 0°. The measured momentum distribution of the ^{3}He particles was used to determine the Q value spectrum in the region -145 MeV $< Q < -120$ MeV with a systematic uncertainty of ± 120 keV and a full width at half maximum resolution of 480 ± 60 keV. This spectrum shows a prominent peak at $Q \simeq -135.5$ MeV, corresponding to the pionic $2p$ state, coupled mainly to the $3p_{1/2}$ and $3p_{3/2}$ neutron hole states in ^{207}Pb. A shoulder is seen on the tail of this dominant peak, and is attributed to the population of the pionic $1s$ state. The cross section for the continuum component at these high excitation energies is $d^2\sigma/(d\Omega dE) = 4.7$ μb/sr MeV. The net cross section for production of π^- states in the bound pion region -140 MeV $< Q < -133$ MeV above the continuum amounts to $d\sigma/d\Omega = 76$ μb/sr.

PACS number(s): 36.10.Gv, 14.40.Aq, 25.45.Hi, 27.80.+w

I. INTRODUCTION

Since their first observation in 1952 [1] pionic atoms have been formed by the capture and subsequent electromagnetic deexcitation of stopped π^-. x rays emitted in the electromagnetic cascade gave experimental access to the determination of the pionic binding energies (see Ref. [2], and references therein). In heavy atoms the electromagnetic cascade stops before reaching the lowest states due to the absorptive part of the strong interaction. States inside the ''last'' orbital, where the x-ray cascade terminates, will be referred to as ''deeply bound pionic states'' in the following. For these states, assuming a pure Coulomb potential and neglecting the contribution of the strong interaction, the calculated probability for the pion being inside the nucleus is comparable or even higher than for being outside. However, the repulsive s-wave part of the strong interaction pushes the pionic wave functions outwards and therefore the pion mainly resides in close vicinity of the nucleus in the potential pocket, which is formed by the repulsive strong interaction together with the attractive Coulomb interaction. In the corresponding halolike states of the π^-, the pion absorption by the nucleus is comparatively low due to the strongly reduced overlap of the pionic density and the imaginary part of the strong interaction. This results in level widths which are still large com-

pared to the electromagnetic widths but small compared to the level distances. The first to recognize this aspect were Friedman and Soff in 1985 [3] and Toki *et al.* in 1988 [4,5]. Instead of widths $\Gamma \simeq 20$ MeV, as expected for complete overlap, widths of $\Gamma \simeq 0.5$ MeV or less are obtained in calculations using the known parameter sets for the optical potential [2,6–10], which are derived by fits to the large amount of experimental data on higher lying levels of pionic atoms and on low-energy π-nucleus elastic scattering.

A special feature, which makes the study of the deeply bound states extremely interesting, is the remarkable sensitivity of their binding energies and widths on the s-wave part of the pion-nucleus potential. This s-wave part, which is directly related to the effective pion mass in the nuclear medium [11], has not been well determined so far.

The standard method for the formation of pionic atoms not being usable for the population of deeply bound pionic states, several alternative methods were proposed, for example, pion transfer reactions, such as (n, p) [5] and (n, d), $(p, {}^2\text{He})$, $(d, {}^3\text{He})$ [12,13]. In the last three reactions, a pionic atom is formed by removing a neutron from the target nucleus and converting it into a (bound) π^- and a proton which is picked up by the projectile. In other theoretical studies it was proposed to populate deeply bound pionic states by (γ, π^+) and (e, e') reactions [14,15], radiative capture of pions in flight (π^-, γ) [16,17], and the decay of hypernuclei [18].

Some of the proposed reactions were already examined

*Electronic address: Hansjoerg.Gilg@Physik.TU-Muenchen.de

experimentally, for instance (n,p) [19] or (π^-,γ) [20], but no clear evidence for the production of deeply bound pionic atoms was found. In the experiments using the (n,d) reaction at TRIUMF [21] and the $(p,{}^2\text{He})$ reaction at RCNP [22] an enhanced yield was observed below the threshold for free π^- production, but no discrete states were identified.

Recently deeply bound $\pi^- \otimes {}^{207}\text{Pb}$ states were discovered in an experiment at the GSI fragment separator, using the ${}^{208}\text{Pb}(d,{}^3\text{He})$ reaction. A short description of the experiment including first results was already published [23], and some implications on the effective pion mass in the nuclear medium were discussed [24]. The aim of the present paper is to describe the experimental requirements (Sec. II) and setup (Sec. III) as well as the necessary calibration measurements (Sec. IV) in detail, and to present its final results (Sec. V). In a succeeding paper [25] the experimental results will be analyzed in detail in order to deduce the binding energies and widths, which will be discussed in their relation to the pion-nucleus interaction. Detailed description of the spectrometer system used in the experiment will be given elsewhere [26].

II. PRINCIPLES AND EXPERIMENTAL REQUIREMENTS

Since a (n,d) reaction experiment on ${}^{208}\text{Pb}$ at $T_n = 400$ MeV at TRIUMF [21] indicated the presence of quasifree π^- production and some bound component, we were encouraged to use the $(d,{}^3\text{He})$ reaction which promised an improvement of both resolution and yield. Elaborate theoretical studies of the (n,d) and $(d,{}^3\text{He})$ reactions were developed by Toki *et al.* [12,13]. Compared to the other reactions used so far, the $(d,{}^3\text{He})$ reaction combines several advantages. The most important ones are as follows.

(i) Relatively large cross sections for the population of deeply bound states are predicted. In the effective number approach this cross section is written as [12,13]

$$(d\sigma/d\Omega)_{dA\to{}^3\text{He}(A-1)\pi} = (d\sigma/d\Omega)^{\text{lab}}_{dn\to{}^3\text{He}\pi} N_{\text{eff}}. \quad (2.1)$$

Since in the $(d,{}^3\text{He})$ reaction, the ejectile is heavier than the projectile, there exists a so called "magic" incident energy, where the momentum transfer (and hence the angular momentum transfer ΔL) is zero. Around this incident energy ($T_d \simeq 250$ MeV/nucleon), the effective numbers N_{eff} for the formation of quasisubstitutional states [states with $\Delta L = 0$ such as $(p_{3/2,1/2})_n^{-1}(2p)_\pi$] are strongly enhanced. Additionally, the elementary cross section $(d\sigma/d\Omega)_{dn\to{}^3\text{He}\pi}$ is peaked at $T_d \simeq 300$ MeV/nucleon, close to the "magic" energy.

(ii) The deuteron projectile is charged and is available as a primary beam. Therefore, the requirements on intensity and momentum spread of the beam can be accomplished much more easily than e.g., in the case of (n,d).

(iii) In comparison to the reactions which require the detection of two particles in the exit channel [e.g., $(d,2p)$], the demands on momentum and angular acceptance are strongly reduced.

In the present experiment we decided to use $T_d = 300$ MeV/nucleon to observe enhanced formation of the $2p$ states of π^-. In order to use the advantages of the

$(d,{}^3\text{He})$ reaction for the formation of the deeply bound states, several essential requirements have to be fulfilled.

(1) For clear separation of the different states an overall energy resolution of $\Sigma_Q \simeq 0.5$ MeV [full width at half maximum (FWHM)] is required. Since the Q value is determined by the difference of the kinetic energies of ejectile and projectile ($T_{{}^3\text{He}} \simeq 470$ MeV, $T_d \simeq 600$ MeV; the energy of the recoiling ${}^{207}\text{Pb}$ nucleus is only $T_{{}^{207}\text{Pb}} \simeq 8$ keV and may be neglected) the energy spread of the incident beam ($\delta T_d/T_d$) and the resolution of the spectrometer ($\delta T_{{}^3\text{He}}/T_{{}^3\text{He}}$) have to be noticeably better than 10^{-3}.

(2) A large momentum acceptance $\Delta p/p = \pm 0.6\%$ is required for the ejectile so as to cover the bound pion region $E_x = 130$–140 MeV.

(3) For kinematical reasons a low momentum transfer can only be achieved if the ${}^3\text{He}$ ejectile is emitted at an angle close to $0°$ with respect to the direction of the incident beam. At larger angles the increasing momentum transfer leads to a strongly decreasing differential cross section for the production of deeply bound states. At $\Theta_{1/2} \simeq 1.3°$ the differential cross section for the $(p_{3/2})_n^{-1}(2p)_{\pi^-}$ state in ${}^{207}\text{Pb}$ is already reduced by a factor of 2 [13]. Therefore the measurement requires a $0°$ spectrometer which can separate the ${}^3\text{He}$ particles produced in the target from the primary beam well.

(4) The measurement at an angle of $0°$ requires particular caution in the suppression of background produced by the primary beam when hitting material other than the target. Two possible sources for this kind of background may affect the measurement of the ${}^3\text{He}$ momentum spectrum from the ${}^{208}\text{Pb}(d,{}^3\text{He})$ reaction.

(a) High count rates of d projectiles suffering energy loss and/or scattering in the inner wall of the spectrometer magnet where the beam is dumped; this background might overload the detection system.

(b) ${}^3\text{He}$ particles from $(d,{}^3\text{He})$ reactions originating from the same location, which can only be suppressed due to their different trajectories.

For sufficient suppression of these background contributions a spectrometer system composed of two or more bending sections is required.

(5) In addition, the Coulomb breakup of deuterons in the ${}^{208}\text{Pb}$ target causes a huge proton background, which peaks at a magnetic rigidity close to the one for the ${}^3\text{He}$ particles to be investigated [27]. In the region of magnetic rigidity corresponding to the population of deeply bound states, we expected a proton rate, which exceeds the rate of ${}^3\text{He}$ by a factor of $\simeq 5 \times 10^4$. It is essential to suppress these background events which would overload the detection systems.

III. EXPERIMENTAL SETUP AND PARTICLE IDENTIFICATION

In order to fulfill the requirements listed in the previous section, the experiment was performed using the GSI fragment separator. The heavy ion synchrotron SIS supplied a deuteron beam with the required energy of $T_d = 604.3$ MeV (magnetic rigidity $B\rho = 5.413$ Tm) and a momentum spread of $\delta p/p < 4 \times 10^{-4}$ which is sufficient for the aspired Q value resolution. Since the available beam intensity is high
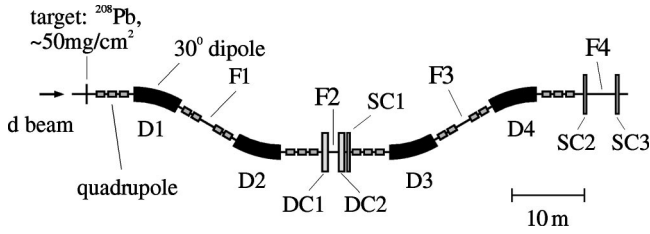
FIG. 1. Experimental setup at the GSI fragment separator. At the focal planes $F2$ and $F4$ drift chambers (DC1, DC2) and scintillators (SC1, SC2, SC3) were positioned. Of the 36 FRS magnets only the dipoles ($D1$, $D2$, $D3$, $D4$) and the quadrupoles are shown, and hexapoles and Y steering magnets are omitted. The target and the detectors are not shown to scale.

enough (up to 10^{11} per acceleration cycle), a thin target (thickness $\simeq 50$ mg/cm^2) could be used so that its contribution to the energy resolution could be kept within the required limits. The duration of the acceleration cycle was 2.8 s, of which about 1 s was used for the extraction of the beam.

In addition to the characteristics of the ion beam the high resolving power and the good background suppression capability of the fragment separator (FRS) [28] were of equal importance for the experiment. The FRS can be used as a high resolution magnetic spectrometer, which is able to separate the ^{3}He particles emitted at 0° from the primary beam and measure their momenta with sufficient precision. The fragment separator consists of four symmetric bending sections with different bending directions (Fig. 1). It therefore guarantees the required background suppression. Every section is composed of a dipole magnet with 30° deflection angle, a quadrupole triplet and a quadrupole doublet for beam focusing, and a Y steering magnet. In addition, a hexapole magnet in front and behind each dipole magnet allows us to compensate second order ion optical aberrations. The field of each FRS magnet can be adjusted individually. Detectors were placed at two of the focal planes ($F2$ and $F4$).

The first half of the FRS was used to measure the momentum distribution of the ^{3}He particles produced in the target, from which the Q value spectrum can be deduced. For this purpose the particle position at the dispersive focal plane $F2$ was determined by means of two sets of drift chambers, which were built for the present purpose. These detectors, originally developed for (π^+,K^+) spectroscopy at KEK [29], with an active area of 24 cm(horizontal) $\times$ 14 cm(vertical), had a small drift cell size (5 mm) so that they allowed for high counting rates of up to several 10^6/s. Therefore it was no problem to cope with the singles rates at $F2$, which were typically $<10^5$/s and $\simeq 2 \times 10^5$/s (mainly protons) in the measurements with ^{208}Pb target and $(CH_2)_n$(=polyethylene) target, respectively. In addition to the position in the direction of dispersion (x) and in the perpendicular direction (y) also the angles of the particle trajectory in both directions (Θ_x, Θ_y) were measured. Thus in the data analysis higher order ion optical aberrations could be corrected, improving the Q value resolution considerably.

In order to avoid a reduction of the momentum resolution, no matter (detectors, degrader material) was placed in the
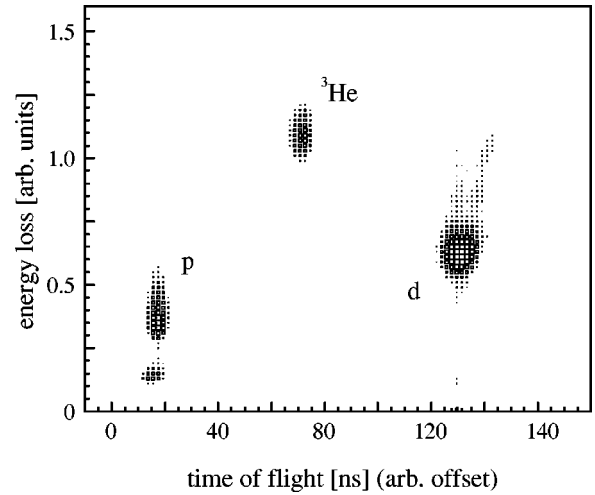

FIG. 2. Correlation of energy loss in the scintillator SC2 and time of flight from the central to the final focal plane, determined in a measurement with ^{208}Pb target. The flight path between both focal planes has a length of $\sim$36 m. Protons, deuterons, and ^{3}He particles are clearly separated.

beam between the target and $F2$. As a consequence the drift chambers were exposed to the full background of protons from deuteron breakup and of scattered deuteron projectiles transmitted to $F2$. The suppression of this background and the identification of ^{3}He was only possible in the second half of the FRS, behind the position measurement at $F2$. For particle identification, scintillation detectors were placed at the focal planes $F2$ (SC1) and $F4$ (SC2 and SC3). In order to avoid overload effects due to the high proton background the start detector at $F2$ (SC1, width: 240 mm, height: 94.5 mm) was segmented into eight horizontal strips. The scintillation detectors delivered three energy loss signals and two independent time of flight signals. A part of this information was already sufficient for unambiguous particle identification. The analysis conditions for the ^{3}He spectra shown in this paper use the time of flight (TOF) between the scintillator at $F2$ (SC1) and the first scintillator at $F4$ (SC2) as well as the energy loss signals of both detectors, but even in a two-dimensional plot of one TOF versus one energy loss signal the different particle species are clearly separated, as shown in Fig. 2. On the other hand, the possibility to identify the particles using only the signals of the detectors at $F4$ was very helpful to determine the efficiency of the detectors at $F2$.

The proton background from deuteron breakup was very much reduced due to the different energy loss of protons and ^{3}He in the material which the particles had to pass at $F2$, mainly the scintillator SC1, simultaneously serving as a degrader. The energy loss in this material (thickness $\simeq$1.7 g/cm^2) results in a change in the magnetic rigidity $B\rho$, which depends on the particle species ($\Delta B\rho = 0.0270$ Tm for protons, 0.1071 Tm for deuterons, and 0.1144 Tm for ^{3}He). The central $B\rho$ value of the FRS sections 1 and 2 was $B\rho = 2.799$ Tm (in an ion optical setting for 1678 MeV/c central momentum of ^{3}He), whereas the setting of the FRS sections 3 and 4 was adjusted to the $B\rho$ value of the ^{3}He particles after passing the material ($B\rho = 2.685$ Tm). Thus about 80%

TABLE I. Targets used to investigate the ^{208}Pb$(d,^3$He$)$ reaction and to perform calibration measurements. The diameter of the targets was $\simeq 20$ mm, which is large compared to the size of the beam spot (1–2 mm).

Number	Material	Thickness (mg/cm^2)	Shape	Purpose
1	^{208}Pb	45.2 ± 0.5	stripe width: 2.0 mm	^{208}Pb$(d,^3$He$)$ reaction: Q value spectrum
2	$($CH$_2)_n$	55.6 ± 0.5	stripe width: 2.0 mm	Q value calibration
3	^{208}Pb	50.5 ± 0.5	full	^{208}Pb$(d,^3$He$)$ reaction: cross section
4	^{9}Be$(+$Nb$)$	1022 ± 9 $(+221.3 \pm 2.0)$	full	determination of acceptance function
5	^{27}Al	35 ± 1	stripe width: 2.0 mm	^{27}Al$(d,^3$He$)$ reaction: Q value spectrum
6	^{27}Al	805 ± 10	hole target hole diameter: 1.0 mm	ion optics, Q value resolution

of the ^{3}He particles that reached $F2$ were transmitted to the focal plane $F4$. For protons the change of the magnetic rigidity is much smaller. Only a very small fraction of protons reached $F4$ and therefore the total counting rate at the final focal plane was only $\simeq 500$/s. The transmitted particles were detected by the two scintillators (SC2 and SC3) placed at $F4$. The low counting rate at $F4$ allowed for the generation of a selective ^{3}He trigger. Only when a signal of the scintillator SC1 (at $F2$) above the threshold for ^{3}He particles was coincident to a signal of the scintillator SC2 (at $F4$), the data acquisition was triggered and the corresponding event was written to tape.

In conclusion, due to the redundant procedures for the particle identification there was no contaminant in the ^{3}He data sample. Due to the two-step bending at $D1$ and $D2$, the reaction products emerging from the inner wall of the first dipole magnet $D1$, where the primary beam was stopped, did not affect the measurement. In a run without target, the total particle rate was low compared to the runs with a target and no substantial ^{3}He background of instrumental origin was observed. The targets used to determine the Q value spectrum and the cross section of the ^{208}Pb$(d,^3$He$)$ reaction and to perform the necessary calibration measurements are shown in Table I.

IV. CALIBRATION MEASUREMENTS

A. Q value calibration of the spectrometer using the reaction $p(d,^3$He$)\pi^0$

To determine the Q value in a ^{208}Pb$(d,^3$He$)\pi^- \otimes {}^{207}$Pb reaction we had to measure the difference of the kinetic energies of ejectile ($T_{^3\text{He}} \simeq 470$ MeV) and projectile ($T_d = 604.3$ MeV). The kinetic energy of the produced pionic atom is $T_{\pi \otimes \text{Pb}} \simeq 0.008$ MeV and therefore negligible. The Q value is related to the excitation energy E_x, which we define with respect to the ground state of ^{207}Pb as

$$-Q = E_x + S_n(p_{1/2}) - [M_n + M_d - M_{^3\text{He}}]c^2 = E_x + 0.58 \text{ MeV},$$
$$(4.1)$$

where $S_n(j_n)$ is the neutron separation energy $[S_n(p_{1/2}) = 7.37$ MeV, for the $(3p_{1/2})_n^{-1}$ state]. The binding energy B_π of the π^- for a ^{207}Pb nucleus being in the ground state $[(3p_{1/2})_n^{-1}]$ is then [25]

$$B_\pi = m_{\pi^-}c^2 - E_x = Q + 140.15 \text{ MeV}. \qquad (4.2)$$

If the ^{207}Pb nucleus is in an excited $(nlj)_n^{-1}$ state

$$B_\pi = m_{\pi^-}c^2 - E_x + E_n(nlj) = Q + 140.15 \text{ MeV} + E_n(nlj),$$
$$(4.3)$$

where $E_n(nlj)$ is the excitation energy of the neutron hole state in ^{207}Pb. Therefore the error in the binding energy is identical to the error in the Q value. Consequently, to achieve the desired precision of $\delta B_\pi \lesssim 0.2$ MeV, the difference of the kinetic energies of projectile and ejectile had to be determined with the same precision.

The appropriate accuracy for the Q value calibration of the FRS spectrometer was attained using the $p(d,^3$He$)\pi^0$ reaction on a $($CH$_2)_n$ $(=$polyethylene$)$ target, which produces a monoenergetic peak. This method provides a built-in calibration for the energy difference $(T_d - T_{^3\text{He}})$, which is determined by a factor 10 more precisely than the absolute values of T_d and $T_{^3\text{He}}$ are known. From the masses of the relevant particles $m_p = 938.2723$ MeV/c^2, $m_d = 1875.6133$ MeV/c^2, $m_{^3\text{He}} = 2808.3921$ MeV/c^2, $m_{\pi^0} = 134.9764$ MeV/c^2, and $m_{\pi^-} = 139.5700$ MeV/c^2 [30,31] the Q value of the reaction $Q = -129.483$ MeV is known to a precision of $\delta Q < 1$ keV. At fixed projectile energy the kinetic energy of the ^{3}He ejectile depends only on the emission angle. For an incident energy of $T_d = 604.3$ MeV and emission in beam direction an ejectile energy of $T_{^3\text{He}} = 463.5$ MeV is obtained. This value is close to $T_{^3\text{He}} = 464.1$ MeV, the ejectile energy in the ^{208}Pb$(d,^3$He$)\pi^- \otimes {}^{207}$Pb reaction corresponding to the threshold for quasifree π^- production ($Q = -140.15$ MeV). In the FRS angular acceptance range $(\Delta x' \simeq \pm 9$ mrad, $\Delta y' \simeq \pm 5.5$ mrad) approximately monoenergetic ^{3}He particles were observed, showing a narrow peak in the position spectrum of these
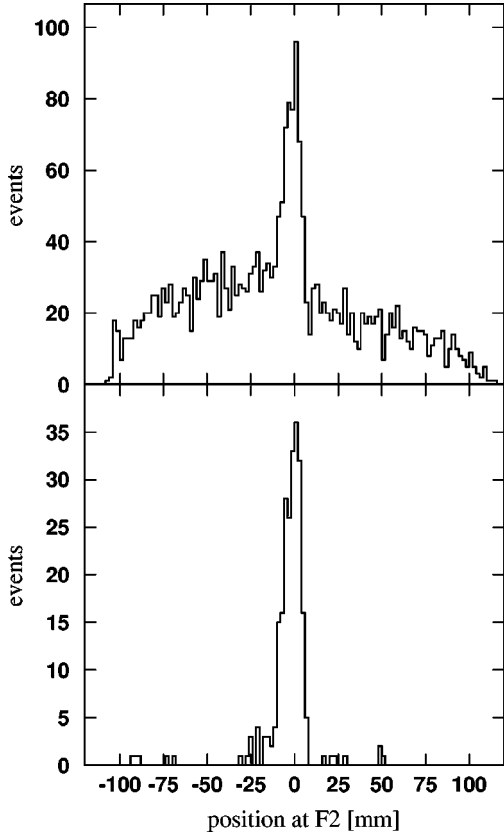
FIG. 3. Position spectrum at the central focal plane $F2$ in a measurement using a $(CH_2)_n$ target. In the upper figure, where ^{3}He particles are selected only by the energy loss signal of the scintillator SC1 at $F2$, a considerable flat continuum appears. In the lower figure with full particle identification—also using the information from scintillator SC2 at $F4$—such background disappears completely, leaving a very low level continuum arising from the ^{12}C$(d,^3$He$)$ reaction.

particles at the central focal plane $F2$, as illustrated in Fig. 3. In the further analysis a correction for the small dependence of the ejectile energy on the emission angle (at an angle of $\theta=9$ mrad the kinetic energy of the ^{3}He particle is reduced by 0.45 MeV compared to $\theta=0$ mrad) was taken into account.

The Q value calibration of the fragment separator was performed by determining the position of the peak for a given magnetic field setting. In a series of measurements the FRS was adjusted to several slightly differing central momenta by scaling the fields of all magnets using a common factor. In this way the position of the peak was shifted across the central focal plane $F2$ covering the full acceptance. A linear relation of central momentum and peak position was found, from which a momentum dispersion of $dx/d(\delta p/p) = (-6.848 \pm 0.012)$ cm/% at $F2$ was deduced. This corresponds to an energy dispersion of $dx/d(\delta E/E) = (-26.03 \pm 0.046)$ cm/% in the selected momentum range. This experimental value is in good agreement with the one obtained in a calculation using the ion optical code GICO [32], $dx/d(\delta p/p) = -6.8864$ cm/%.

For the three different magnetic settings of the fragment separator (optical settings A,B,C, corresponding to ^{3}He mo-

menta of 1678, 1688, and 1696 MeV/c in the center of the focal plane) which were used for the measurements with the ^{208}Pb target, the ^{3}He produced in the $p(d,^3$He$)\pi^0$ reaction was within the momentum acceptance. Therefore it was possible to perform a calibration measurement with $(CH_2)_n$ target after each change in the FRS setting. From the position of the ''calibration peak'' the central momentum of the corresponding setting could be determined with substantially higher precision than from the measured currents of the magnets or from the magnetic field measurements using Hall probes. To assure the Q value calibration and resolution not to be deteriorated by long term shifts in the magnetic fields (for instance, caused by drifts in the power supplies), this calibration measurement was repeated about every two hours. Whereas the position of the calibration peak was stable at fixed magnetic setting, a significant shift of the peak was observed after having changed the setting, when the original setting was reestablished. Taking into account this effect the resolution was improved considerably.

A difference in the mean energy loss in the $(CH_2)_n$ and in the ^{208}Pb target results in a shift in the Q value scale which had to be considered. For both targets the energy loss of a deuteron ΔE_d and a ^{3}He particle $\Delta E_{^3He}$ was calculated using the code ATIMA [33], and the average of these values was determined. In the case of the $(CH_2)_n$ target the kinematical dependence of the ejectile energy on the projectile energy $(dE_{ejectile}/dE_{projectile}=0.907)$ was taken into account by using the formula

$$\Delta E_{average} = 0.5 \times \left(\Delta E_{^3He} + \frac{dE_{ejectile}}{dE_{projectile}} \Delta E_d \right) \quad (4.4)$$

for averaging. For the lead target $dE_{ejectile}/dE_{projectile}=1$ due to the large mass of the lead nucleus. For the 45.2 mg/cm^2 ^{208}Pb target $\Delta E_{^3He}=0.4812$ MeV, $\Delta E_d=0.0816$ MeV, $\Delta E_{average}=0.2814$ MeV, and for the 55.6 mg/cm^2 $(CH_2)_n$ target $\Delta E_{^3He}=1.265$ MeV, $\Delta E_d=0.207$ MeV, $\Delta E_{average}=0.726$ MeV. Since the kinetic energy of the ^{3}He ejectiles depends on the emission angle, it had to be guaranteed that the particles used for calibration were emitted exactly in the beam direction at the target. Therefore a measurement using the attenuated primary beam was performed in order to determine in which direction a particle emitted at 0° traverses the focal plane $F2$. To make sure that a possible change in the primary beam direction during the experiment could not affect the regularly performed calibration measurements with CH$_2$ target, the beam direction was controlled several times—especially after beam losses—by means of two current grids placed upstream of the target.

B. Precision of the Q value calibration

The uncertainty of the Q value calibration and thus the systematic error in the binding energies of the deeply bound pionic states is affected by several contributions. The following contributions are the dominant ones:

Beam energy. From the circumference of the heavy ion synchrotron SIS [(216.72 ± 0.03) m] and the measured revolution frequency of the beam ($f=904.9405$ kHz) a beam en-

ergy of $T_d = (604.254 \pm 0.257)$ MeV was deduced. The uncertainty in the beam energy of $\delta T_d = \pm 0.257$ MeV, originating mainly in uncertainty of the circumference, leads to an error in the Q value scale of $\delta Q = 0.024$ MeV when the $p(d,{}^3\text{He})\pi^0$ reaction is used for calibration.

Energy loss in the target. The uncertainties in the target thickness, which was measured before the experiment ($\simeq 1\%$), and in the calculation of the energy loss using the code ATIMA [33] ($<3\%$) [34] correspond to errors of $\delta Q \simeq 0.01$ MeV and $\delta Q < 0.0286$ MeV, respectively. After the experiment the targets were inspected and a dark spot was found on the $(\text{CH}_2)_n$ target in the region where it had been hit by the beam. To quantify how the energy loss was changed by this radiation damage, the energy loss of 20 MeV protons in this target was determined at the Munich tandem accelerator laboratory. The Q3D magnetic spectrometer existing there was used to measure the momenta of protons which had passed the target as well as of protons which had not passed it. Whereas on a position beside the spot the measured energy loss of 1.652 MeV agrees very well with the calculation, on the beam spot the energy loss was increased by 7.4% (0.122 MeV). In the Q value calibration measurement using the CH_2 target an increase of 7.4% in the energy loss corresponds to a shift in the Q value scale of 0.054 MeV. To consider this effect the Q value scale was shifted by half of this amount (0.027 MeV) and in the systematic error an additional contribution of $\delta Q = 0.027$ MeV is taken into account.

Emission angle of ^{3}*He.* For kinematical reasons the energy of the ^{3}He particle produced in the $p(d,{}^3\text{He})\pi^0$ reaction depends on its emission angle. Therefore, inaccuracies in the measurement of this angle affect the Q value calibration. The error of the angle mainly originates from the determination of the primary beam direction by means of the current grids and was estimated to be $\delta\varphi \simeq 2$ mrad, which corresponds to an uncertainty in the Q value calibration of $\delta Q \simeq 0.016$ MeV.

Dispersion at the central focal plane. When deeply bound pionic states are produced in the ${}^{208}\text{Pb}(d,{}^3\text{He})$ reaction, the kinetic energy of the ^{3}He particle is approximately 4–8 MeV above the calibration peak. Therefore an extrapolation is necessary, which requires the precise knowledge of the dispersion at the central focal plane $F2$. The experimental uncertainty of $\Delta[dx/d(\delta p/p)] = \pm 0.012$ cm/% causes an error in the Q value calibration of $\delta Q \simeq 0.013$ MeV.

The linear summation of all of these contributions provides a value for the systematic error of the Q value calibration of $\delta Q = 0.12$ MeV.

C. Energy resolution

In order to improve the experimental resolution several calibration measurements were performed. In these measurements higher order ion optical aberrations of the FRS spectrometer as well as the dependence of the beam energy on the time within the extraction cycle were determined. The obtained information was used in the offline analysis to apply appropriate corrections. Thus the resolution has been improved considerably compared to the results of a first analysis of the data [23]. The corrections are described in detail in Ref. [26].

In the following the various contributions to the Q value resolution are presented. However, a part of them could not be measured separately and therefore only upper limits for these contributions can be given.

Energy spread of the beam. For a calibration measurement using an aluminum hole target (thickness 800 mg/cm^2, hole diameter 1 mm) the primary beam intensity was reduced and the FRS magnet setting was adjusted to the magnetic rigidity of the beam particles (deuterons, $T_d = 300$ MeV/nucleon $= 604.3$ MeV). The particles passing the aluminum outside the hole were identified by their energy loss in the target and were rejected in the analysis. For the deuterons passing through the hole the position distribution at the dispersive focal plane $F2$ was determined. From the width of this distribution an energy resolution (after correcting for the time dependence of the beam energy) of $\Delta E = 0.32$ MeV (FWHM) was deduced. Of course, this value also includes contributions due to beam width at target position, position resolution of drift chambers and short term ($t \lesssim 30$ min) fluctuations of the FRS magnetic fields. In contrast higher order ion optical corrections are negligible due to the small phase space of the primary beam compared to the FRS acceptance. Consequently the energy spread of the primary beam causes a contribution $\Sigma_Q < 0.32$ MeV (FWHM) to the Q value resolution.

Beam width at target position. The contribution due to the finite width of the beam was limited by using a 2 mm wide strip target. Applying the position magnification $[(x|x) = 1.22]$ and momentum dispersion $[(x|\delta p) = -6.89$ cm/%$]$ of the FRS setting an upper limit of $\Sigma_Q = 0.31$ MeV (rectangular shape) for this contribution is calculated. The corresponding standard deviation is $\sigma_Q = 0.31$ MeV$/\sqrt{12} = 0.089$ MeV.

Target thickness. Because of the difference in energy loss between deuteron projectile and ^{3}He ejectile the kinetic energy of a ^{3}He particle depends on the depth in the target where the reaction occurred. For the target thickness of 45.2 mg/cm^2 an energy loss calculation yields $\Sigma_Q = 0.40$ MeV (rectangular shape) for this contribution. This value corresponds to a standard deviation of $\sigma_Q = 0.12$ MeV.

Stability of the FRS magnetic fields. Between the regularly repeated calibration measurements (Sec. IV A) the position of the calibration peak changed by less than $\delta x \simeq 1$ mm. Therefore, long term ($t \gtrsim 30$ min) fluctuations of the magnetic fields contribute with $\Sigma_Q \lesssim 0.1$ MeV to the resolution.

Higher order ion optical aberrations. In the data analysis ion optical corrections up to third order were applied. In the determination of these correction terms no hints were found for higher order aberrations that would affect the resolution significantly. These contributions should be negligible compared to the already listed ones.

Position resolution of the drift chambers. The achieved position resolution $\Delta x < 370$ μm corresponds to a value $\Sigma_Q < 0.05$ MeV (FWHM) and is therefore almost negligible.

Unfortunately, the large thickness of the $(CH_2)_n$ target (55.6 mg/cm^2, optimized for high ^{3}He yield in the calibration measurements) does not allow to determine the Q value resolution function from the width of the $p(d,^3$He$)$ calibration peak, since the width is dominated by the energy loss in the target (rectangular shape, full width $\Sigma_Q = 1.077$ MeV), which is larger than that in the ^{208}Pb target. However, a good estimation of the resolution is certainly obtained by considering the contributions due to the energy spread of the beam (approximated by a Gaussian of width FWHM$=0.32$ MeV) and target thickness (rectangular function, full width $\Sigma_Q = 0.40$ MeV). Quadratic addition of the corresponding standard deviations provides a lower limit $\sigma_Q = 0.178$ MeV (FWHM$=0.42$ MeV) for the value of the obtained resolution. This value is required to determine an upper limit for the widths of the deeply bound states and includes almost all essential effects, only the items ''stability of the FRS magnetic fields'' and ''higher order ion optical aberrations'' are not taken into account and the contribution due to the beam width at the target position is possibly slightly underestimated. A safe estimation of these contributions leads to an upper limit of $\sigma_Q = 0.229$ MeV (FWHM$=0.54$ MeV) for the achieved Q value resolution.

D. Acceptance function

In order to determine the shape of the Q value spectrum and the production cross sections from the position distribution of the ^{3}He particles at the central focal plane, the FRS acceptance as a function of the particle momentum and angle must be known. The acceptance function was determined in Monte Carlo simulations [26] using the code MOCADI [33]. To check the simulation results experimentally, a thick ^{9}Be target (thickness$=1022$ mg/cm^2) was irradiated with the deuteron beam ($T_d = 300$ MeV/nucleon) and the momentum distribution of ^{3}He particles emitted in the beam direction was analyzed. The magnetic field setting of the FRS was equivalent to the setting used for the measurements with the ^{208}Pb target but scaled to a central momentum of $p_{^3\text{He}} = 1850$ MeV/c. At this ejectile momentum the excitation energy of ^{8}Li nuclei produced in the ^{9}Be$(d,^3$He$)^8$Li reaction is approximately 25 MeV. It is safe to assume that the differential cross section for production of ^{3}He is flat within the angular acceptance of the FRS spectrometer ($\Delta x' \simeq 18$ mrad, $\Delta y' \simeq 11$ mrad). Since for the ^{3}He particles a flat momentum distribution is expected at these high excitation energies, the measured momentum spectrum should reflect the acceptance function of the spectrometer. The experimental momentum distribution confirms the results of the Monte Carlo simulation for the FRS acceptance (Fig. 4).

E. Q value spectrum for the ^{27}Al$(d,^3$He$)$ reaction

A reference run with a ^{27}Al target was performed, in order to verify that the setup worked properly and instrumental effects were not the origin of the observed structure in the momentum spectrum of the ^{3}He particles in the ^{208}Pb$(d,^3$He$)$ reaction. Due to the low Z ($Z=13$) of aluminum, no formation of deeply bound states is expected for this target material.
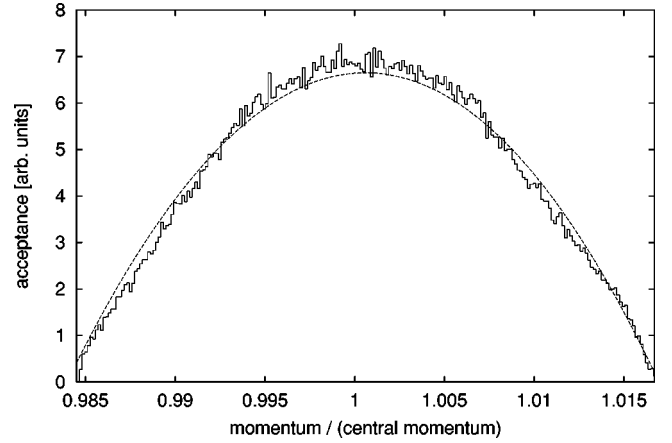

FIG. 4. Momentum acceptance of the FRS spectrometer. The acceptance function obtained in a Monte Carlo simulation (dashed) is in good agreement with the results of the measurement using a ^{9}Be target (fully drawn histogram).

In the ^{27}Al$(d,^3$He$)$ reaction, the threshold for quasifree π^- production is $Q = -145.8$ MeV. At a beam energy of $T_d = 604.3$ MeV this Q value corresponds to an ejectile momentum of $p_{^3\text{He}} = 1668.7$ MeV/c. The FRS magnet setting was scaled to this momentum, but otherwise identical to the settings used in the runs with ^{208}Pb target (optical settings A,B,C). The 2 mm wide strip target had a thickness of 35 mg/cm^2, similar to the thickness of the lead target (45.2 mg/cm^2).

Figure 5 shows the Q value spectrum which reveals a rising yield above the threshold for quasifree π^- production (in the region $Q < -145.8$ MeV), whereas below the threshold a flat continuum is observed. Particularly, there is no signal close to the threshold, which could be a hint for bound states of π^-. This is in agreement to the expectations, and confirms that an observed structure in the Q value spectrum of the ^{208}Pb$(d,^3$He$)$ reaction (Sec. V B) corresponds to the population of deeply bound pionic states.
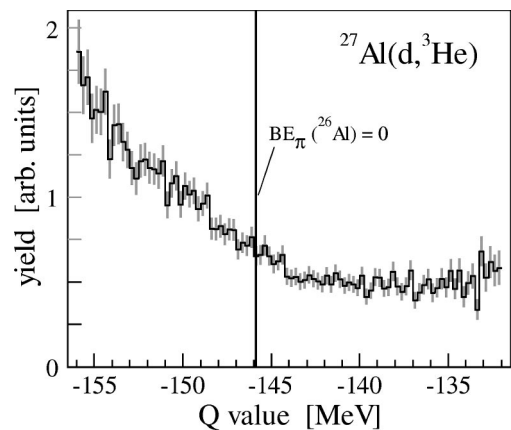

FIG. 5. Q value spectrum of the ^{27}Al$(d,^3$He$)$ reaction. Quasifree π^- production leads to an increasing ^{3}He yield above the threshold for this process ($Q < -145.8$ MeV, indicated by the vertical line). Below the threshold, a smooth continuum is observed.

V. RESULTS

A. Cross section for the ^{208}Pb(d,^{3}He) reaction

In order to determine the cross section for the ^{208}Pb(d,^{3}He) reaction, several comparatively short measurements with a full ^{208}Pb target (thickness 50.5 mg/cm^2; diameter$\simeq$20 mm, which is sufficiently large to cover the beam spot) were performed. In these measurements a SEE-TRAM (secondary electron transmission monitor [35,36]) was used to monitor the intensity of the primary beam. From the number of ^{3}He particles detected in a 20 MeV wide energy interval around the kinetic energy of the reference particle, the integrated cross section in this energy range was determined. Several effects had to be considered.

Using the scintillators positioned at $F4$ for trigger generation and particle identification, the detection efficiency of the counters placed at $F2$ was determined. In the measurements considered here, the overall efficiency of the complete detector system at $F2$ (drift chambers DC1, DC2, and segmented scintillator SC1) for ^{3}He particles was $\epsilon_{\text{det}}\sim70\%$. For the detectors at $F4$ a detection efficiency close to 100% can be safely assumed.

The deadtime of the data acquisition in these measurements was 5–10%, and consequently the detection efficiency $\epsilon_{\text{acq}}=90$–95%.

To determine the transmission through the FRS the simulation code MOCADI [33] was used. For this simulation an ensemble of particles was assumed, which had a flat angular distribution[1] in the region $-25\,\text{mrad}<\theta_x<25\,\text{mrad}$ and $-15\,\text{mrad}<\theta_y<15\,\text{mrad}$. This is sufficient to cover also the tails of the FRS angular acceptance $[\Delta x'\simeq18\,\text{mrad}$ (FWHM), $\Delta y'\simeq11\,\text{mrad}$ (FWHM)]. The energy distribution of the particle ensemble at the target was chosen according to the experimentally determined, acceptance corrected Q value distribution. For a particle within this ensemble the probability to reach the final focal plane of the FRS is $\tau=31\%$.

The ^{3}He background caused by nuclear reactions in the SEETRAM and in the first FRS dipole magnet—which was used to dump the primary beam—was determined in reference measurements without target and subtracted in the computation of the cross section.

The cross section integrated in the whole energy bite is therefore

$$\frac{d\sigma}{d\Omega}=\left(\frac{N_{\text{Pb}}}{N_{0\text{Pb}}\epsilon_{\text{Pb}}}-\frac{N_{\text{ref}}}{N_{0\text{ref}}\epsilon_{\text{ref}}}\right)\frac{1}{\tau\left(\dfrac{N}{A}\right)_{\text{target}}\Delta\Omega}, \qquad (5.1)$$

where: N_{Pb}, N_{ref} are the number of ^{3}He particles detected in the measurement with Pb target and in the reference measurement, respectively; $N_{0\text{Pb}}$, $N_{0\text{ref}}$ are the number of primary beam particles in these measurements; $\epsilon_{\text{Pb/ref}}$

---

[1]A different simulation, which used a Gaussian angular distribution ($\sigma=19.3$ mrad) to take into account the expected angular dependence of the cross section for production of deeply bound pionic states, gave within a deviation of <9% identical results.
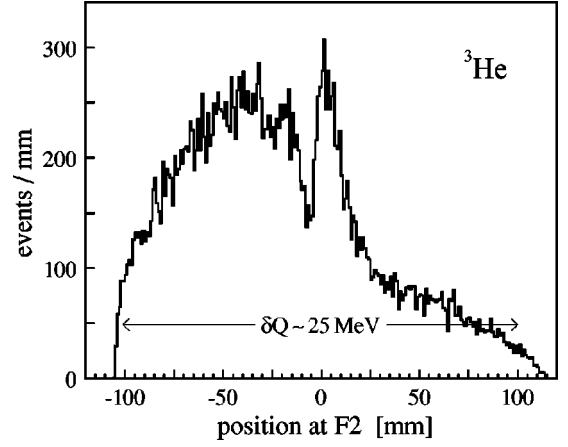

FIG. 6. Position distribution at the central focal plane $F2$ for ^{3}He particles produced in the ^{208}Pb(d,^{3}He) reaction ($T_d=300$ MeV/nucleon). The central momentum is $p=1688$ MeV/c for the FRS magnet setting used here (optical setting B).

$=\epsilon_{\text{det}}\times\epsilon_{\text{acq}}$, where ϵ_{det} is the detector efficiency and ϵ_{acq} the efficiency of the data acquisition in the corresponding measurement; τ is the ion optical transmission through FRS; $(N/A)_{\text{target}}$ is the number of target atoms per area; $\Delta\Omega$ is the solid angle covered by the particle ensemble which was used in the simulation of the transmission ($\Delta\Omega=1.5$ msr).

The systematic error in this measurement is mainly composed of the error in determining the intensity of the primary beam using the SEETRAM ($\sim\pm10\%$) and in the simulation of the transmission through the FRS ($\sim\pm20\%$). The number of events in the measurements with and without target corresponds to a statistical error of 11.8%.

At an angle of 0° the cross section for the reaction ^{208}Pb(d,^{3}He) integrated in the region $-140\,\text{MeV}<Q<-133$ MeV, amounts to

$$\left(\frac{d\sigma}{d\Omega}\right)_{\text{lab}}=109\,\frac{\mu\text{b}}{\text{sr}}(1\pm0.118\pm0.3).$$

A description of the different contributions to the cross section (bound pionic states, quasifree pion production, continuum background), is given in the following section.

B. Q value spectrum of the reaction ^{208}Pb(d,^{3}He)

The measured position distribution of the ^{3}He particles at the dispersive focal plane $F2$ (Fig. 6) was used to determine the Q value spectrum of the reaction ^{208}Pb(d,^{3}He). From the position of a ^{3}He particle relative to the p(d,^{3}He)π^0 calibration peak (Sec. IV A) its momentum and kinetic energy were computed, considering the position and angular dependent ion optical corrections. Assuming a two-body final state, the Q value of the ^{208}Pb(d,^{3}He) reaction can be determined if the beam energy is well known. Here an observed time dependence of the beam energy within one extraction cycle was taken into account in order to improve the resolution. The obtained Q value spectrum was divided by the acceptance function of the corresponding FRS magnetic setting, which was determined in Monte Carlo simulations. Figure 7
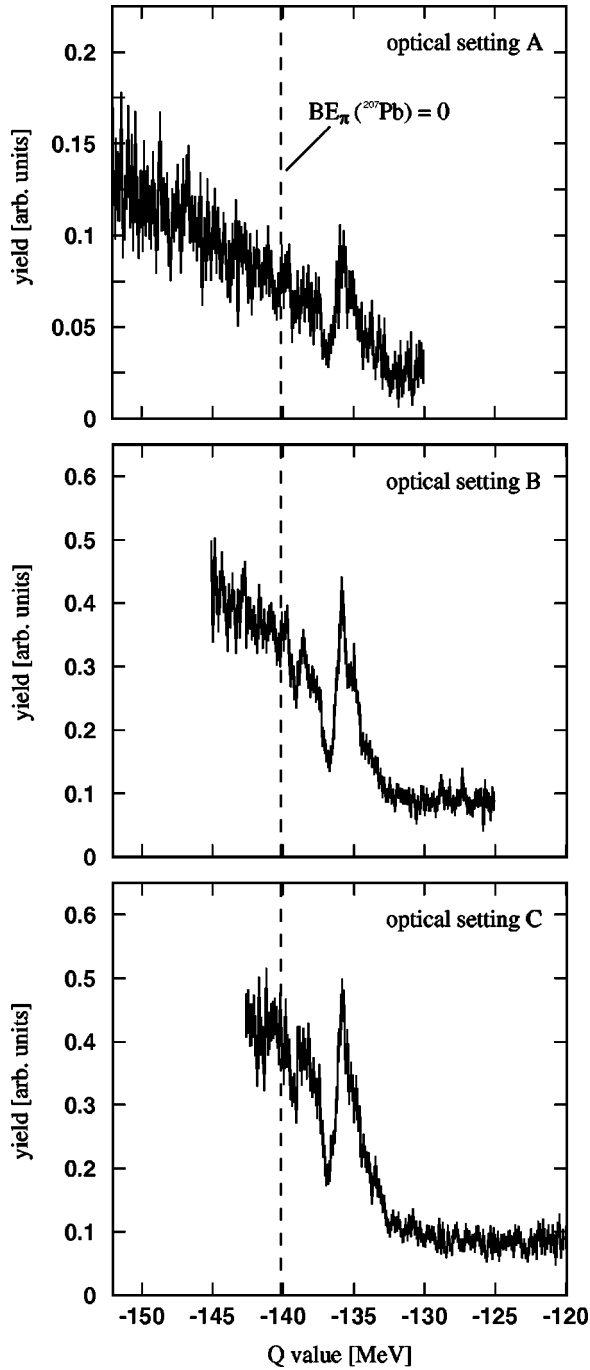
FIG. 7. Acceptance corrected Q value spectra of the reaction ^{208}Pb($d,^3$He) for three different magnetic settings of the fragment separator (optical settings A,B,C). According to the different central momentum slightly different Q value regions are covered. On the right side of the dashed line ($Q > -140.15$ MeV) the production of a free π^- is kinematically not allowed, in this range negative pions can be produced only in the bound state.

shows the acceptance corrected spectra for three different FRS settings (optical settings A,B,C) with slightly different central momenta. Using three different settings allowed covering a wider momentum range as well as excluding possible instrumental effects (e.g., position-dependent detector effi-
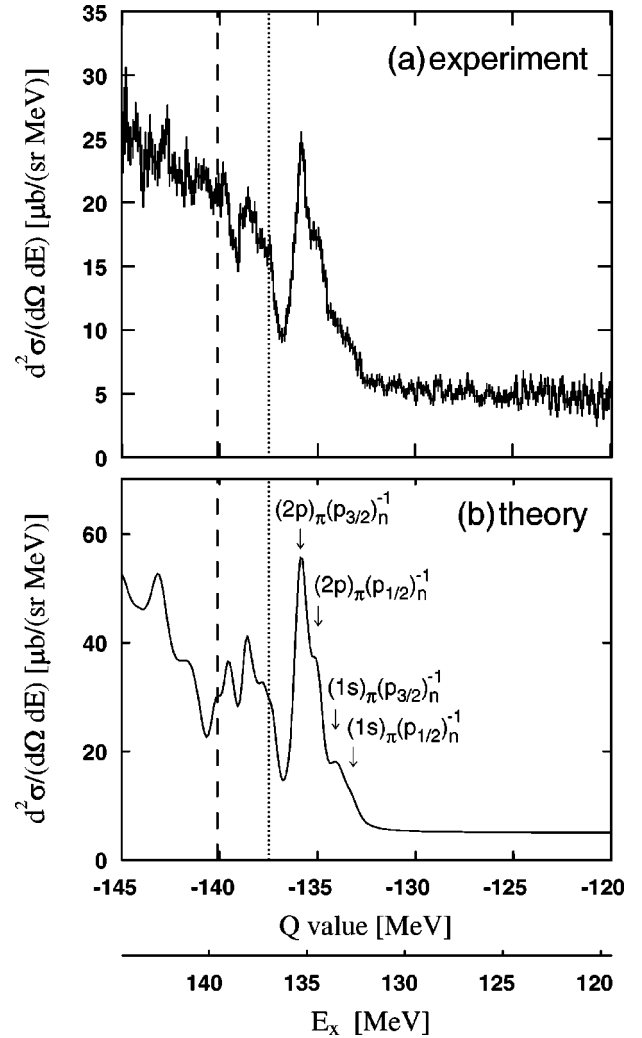

FIG. 8. Experimental Q value spectrum (a) of the reaction ^{208}Pb($d,^3$He), obtained from the spectra for the three FRS settings (optical settings A,B,C) compared to a theoretical calculation (b). Since the threshold for the production of a free π^0 in the ^{208}Pb($d,^3$He) reaction is at $Q = -137.49$ MeV (indicated by the dotted line), there is no contribution due to this process in the region of the dominant peak.

ciencies) to be the origin of the observed structure in the Q value spectrum.

All three Q value spectra have a common shape: Above the threshold for free π^- production ($Q < -140.15$ MeV) a ^{3}He yield increasing to lower Q values is observed. Between $Q = -140.15$ MeV and $Q \simeq -132$ MeV, in the region which corresponds to the expected binding energies of pionic atoms, a clear structure is visible. A peak at $Q \simeq -135.5$ MeV is particularly pronounced. For $Q \gtrsim -132$ MeV a flat distribution of the produced ^{3}He is obtained, as expected at these high excitation energies for background processes which are not related to the production of a pion.

Scaling the three spectra according to the cross section determined in Sec. V A and averaging between the individual data points of the different spectra—taking into account the statistical weights—one obtains the Q value spec-

trum shown in Fig. 8(a). This Q value spectrum is compared with a theoretical calculation in Fig. 8(b). We have made some corrections in the theoretical curve compared to the one shown in Ref. [23]. The previous curve used the elementary pion production cross section $\sigma(n+d\rightarrow{}^3\text{He}+\pi^-)$ at zero degree in the laboratory frame $\sigma(0°)=3.7$ mb/sr. This value is obtained by using the angular distribution of $d+p\rightarrow t+\pi^+$ reactions at 325 MeV/nucleon, where the data was available. In the new calculation shown in Fig. 8(b), the elementary cross section $\sigma(0°)=2.8$ mb/sr is used. This value is obtained by the theoretical work of Fearing [37] on the energy dependence of $d+p\rightarrow t+\pi^+$ cross sections from the $p+p\rightarrow d+\pi^+$ experimental reactions and the normalization to the $d+p\rightarrow t+\pi^+$ experimental cross section in this energy range ($T_d=300$ MeV$\sim$800 MeV) [12]. The second one is related with the correction of a factor 2 in the effective number [12] and with more realistic calculation of N_{eff} using the Woods-Saxon wave functions for the neutron holes. For the detail, see the succeeding paper [25]. In the predicted Q value spectrum [13] a value of $d^2\sigma/(d\Omega dE)=40$ μb/(sr MeV) was used for the expected flat background continuum originating from processes which are not related to the production of a pion. This value was obtained by a simple estimate in which the measured background cross section in the ^{208}Pb(n,d) reaction [21] was scaled by a factor 1/10 according to the calculated ratio of bound π^- formation in $(d,{}^3\text{He})$ compared to (n,d). In spectrum 8(b) the value was changed to $d^2\sigma/(d\Omega dE)=5$ μb/(sr MeV) in order to match our experimental findings.

The experimental spectrum shows a striking agreement to the theoretical prediction [12,13] and to the improved calculation presented in Fig. 8. Comparing both Q value spectra, the experimentally observed dominant peak at $Q\simeq-135.5$ MeV can be attributed to the $(2p)_\pi$ state of pionic ^{207}Pb. This assignment is confirmed by the shape of the peak, which reveals a steep rise at lower Q values, whereas on the side of higher Q values an additional but unresolved component is indicated. The observed skewness of the peak is not of instrumental origin; the $p(d,{}^3\text{He})$ calibration spectrum shows a symmetric shape.

The prediction expects the $(2p)_\pi$ state to be coupled to different neutron hole states in ^{208}Pb $[(3p_{1/2},2f_{5/2},3p_{3/2},1i_{13/2})_n^{-1}]$. According to this prediction the main contribution is due to the quasisubstitutional states $(2p)_\pi(3p_{1/2})_n^{-1}$ and $(2p)_\pi(3p_{3/2})_n^{-1}$, which are separated by 0.897 MeV. Corresponding to the number of neutrons in the $3p_{1/2}$ and $3p_{3/2}$ shell of ^{208}Pb an intensity ratio of 1:2 is expected, which can explain the observed shape of the peak.

A shoulder of the $(2p)_\pi$ peak at higher Q values (more deeply bound states) concurs with the expectations for the $(1s)_\pi$ state coupled to the already listed neutron hole states. In the region between $Q=-139$ MeV and $Q=-136.5$ MeV the experimental spectrum reveals a structure, which is theoretically explained by the population of $(3p)_\pi$ and $(3d)_\pi$ states coupled to $(3p_{1/2},3p_{3/2})_n^{-1}$ neutron hole states.

In the range between $Q=-132$ MeV and $Q=-120$ MeV, the domain of a flat continuum background, a

double differential cross section of $d^2\sigma/(d\Omega dE)=4.7$ μb/(sr MeV) was measured. Assuming the background to be constant across the whole accepted Q value range and subtracting it in the experimental spectrum one obtains a net cross section for the total bound region (-140.15 MeV$<Q<-133$ MeV) $d\sigma/d\Omega=76$ μb/sr, whereas in the region of quasifree pion production (-145 MeV$<Q<-140.15$ MeV) the net cross section amounts to $d\sigma/d\Omega=94$ μb/sr.

In a succeeding paper [25] the obtained spectrum will be analyzed in detail in order to deduce the pionic binding energies and widths, which will be compared to theoretical predictions and discussed in their relation to the pion-nucleus interaction.

VI. CONCLUSION

We have reported the first observation of deeply bound pionic states in an experiment, which investigated the ^{208}Pb$(d,{}^3\text{He})$ pion transfer reaction at a beam energy $T_d=604.3$ MeV and at negative Q values close to the pion mass. The fragment separator at GSI was used as a high resolution magnetic spectrometer to identify the ^{3}He particles emitted at 0° and to measure their momenta. From the ^{3}He momentum distribution the Q value spectrum was determined with a systematic uncertainty $\delta Q\simeq0.12$ MeV in the Q value scale. The lower limit for the value of the resolution in Q was determined to be $\sigma_Q=0.178$ MeV, and a safe estimation leads to an upper limit $\sigma_Q=0.229$ MeV.

Below the threshold for free π^- production the Q value spectrum shows a structure which gives a clear evidence for the population of deeply bound pionic states. The dominant peak at $Q\simeq-135.5$ MeV was attributed to the $(2p)_\pi$ state of pionic ^{207}Pb, coupled to $(3p_{1/2},2f_{5/2},3p_{3/2},1i_{13/2})_n^{-1}$ neutron hole states in ^{207}Pb. A shoulder of this peak concurs with the expectations for the $(1s)_\pi$ state, and a structure in the region between $Q=-139$ MeV and $Q=-136.5$ MeV is theoretically explained by the population of $(3p)_\pi$ and $(3d)_\pi$ states. The net cross section for production of pionic atoms in the region -140.15 MeV$<Q<-133$ MeV was determined to be $d\sigma/d\Omega=76$ μb/sr.

[1] M. Camac, A. D. McGuire, J. B. Platt, and H. J. Schulte, Phys. Rev. **88**, 134 (1952).

[2] C. J. Batty, E. Friedman, and A. Gal, Phys. Rep. **287**, 385 (1997).

[3] E. Friedman and G. Soff, J. Phys. G **11**, L37 (1985).

[4] H. Toki and T. Yamazaki, Phys. Lett. B **213**, 129 (1988).

[5] H. Toki, S. Hirenzaki, T. Yamazaki, and R. S. Hayano, Nucl. Phys. **A501**, 653 (1989).

[6] L. Tauscher, in *Proceedings of the International Seminar on π-Meson Nucleus Interaction*, Strasbourg, 1971, CNRS-Strasbourg (unpublished), p. 45.

[7] C. J. Batty, S. F. Biagi, E. Friedman, S. D. Hoath, J. D. Davies, G. J. Pyle, and G. T. A. Squier, Phys. Rev. Lett. **40**, 931 (1978).

[8] C. J. Batty, E. Friedman, and A. Gal, Nucl. Phys. **A402**, 411 (1983).

[9] R. Seki and K. Masutani, Phys. Rev. C **27**, 2799 (1983).

[10] J. Nieves, E. Oset, and C. Garcia-Recio, Nucl. Phys. **A554**, 509 (1993).

[11] T. Waas, R. Brockmann, and W. Weise, Phys. Lett. B **405**, 215 (1997).

[12] H. Toki, S. Hirenzaki, and T. Yamazaki, Nucl. Phys. **A530**, 679 (1991).

[13] S. Hirenzaki, H. Toki, and T. Yamazaki, Phys. Rev. C **44**, 2472 (1991).

[14] J. Nieves and E. Oset, Phys. Lett. B **244**, 368 (1990).

[15] J. Nieves and E. Oset, Phys. Rev. C **43**, 1937 (1991).

[16] J. Nieves and E. Oset, Phys. Lett. B **282**, 24 (1992).

[17] J. Nieves and E. Oset, Nucl. Phys. **A553**, 595c (1993).

[18] H. Bando, T. Yamazaki, and J. Zofka, Phys. Rev. C **40**, 875 (1989).

[19] M. Iwasaki *et al.*, Phys. Rev. C **43**, 1099 (1991).

[20] K. J. Raywood *et al.*, Phys. Rev. C **55**, 2492 (1997).

[21] A. Trudel *et al.*, TRIUMF E628 experiment, TRIUMF progress report, 1991 (unpublished); T. Yamazaki, Nucl. Phys. **A553**, 221c (1993).

[22] N. Matsuoka, T. Noro, K. Tamura, M. Yoshimura, M. Yosoi, A. Okihana, and T. Yoshimura, Phys. Lett. B **359**, 39 (1995).

[23] T. Yamazaki *et al.*, Z. Phys. A **355**, 219 (1996).

[24] T. Yamazaki *et al.*, Phys. Lett. B **418**, 246 (1998).

[25] K. Itahashi *et al.*, Phys. Rev. C **62**, 025202 (2000), following paper.

[26] A. Gillitzer *et al.* (unpublished).

[27] J. D. Jafar, H. B. Van der Raay, D. G. Ryan, J. A. Stiegelmair, and R. K. Tandon, Nucl. Phys. **A161**, 105 (1971).

[28] H. Geissel *et al.*, Nucl. Instrum. Methods Phys. Res. B **70**, 286 (1992).

[29] T. Fukuda *et al.*, Nucl. Instrum. Methods Phys. Res. A **361**, 485 (1995).

[30] C. M. Lederer and V. S. Shirley, *Table of Isotopes* (Wiley, New York, 1978).

[31] Particle Data Group, L. Montanet *et al.*, Phys. Rev. D **50**, 1173 (1994).

[32] H. Wollnik, Manual for GICO, Universität Giessen, 1990 (unpublished).

[33] T. Schwab, Ph.D. thesis, Universität Giessen, GSI Report No. GSI-91-10, 1991 (unpublished).

[34] C. Scheidenberger (private communication).

[35] C. Ziegler, T. Brohm, H.-C. Clerc, H. Geissel, K.-H. Schmidt, K. Sümmerer, D. J. Vieira, and B. Voss, GSI Scientific Report No. GSI-91-1, 1991 (unpublished), p. 291.

[36] C. Ziegler, Diploma thesis, Institut für Kernphysik TH Darmstadt, 1992.

[37] H. W. Fearing, Phys. Rev. C **16**, 313 (1977).